12-1993

Toward Virtual Digital Mammograms for Research and Training in Tumor Detection

Charles F. Babbs
Purdue University, babbs@purdue.edu

Leslie A. Geddes
Purdue University

Technical note

Toward Virtual Digital Mammograms for Research and Training in Tumor Detection

CHARLES F. BABBS, MD, PhD and LESLIE A. GEDDES, ME, PhD

Biomedical Engineering Center, Purdue University, West Lafayette, IN 47907, USA

December, 1993

Abstract-- Research in the processing, compression, transmission, and interpretation of digital radiographic images requires evaluation of a wide variety of test images, varying in format, in spatial resolution, and in anatomic content. To evaluate the diagnostic performance of observers using novel versus conventional image formats, large numbers of test images containing known abnormalities are required. This report describes a method for creating high resolution, virtual digital mammograms from computational models of the human breast that include branched lobulated ducts and suspensory ligaments embedded in fatty subcutaneous tissue. Breast phantoms may include any of three types of simulated tumors (fibroadenomas, invasive ductal carcinomas, and intraductal carcinomas). Virtual mammograms are generated by computing x-ray transmission through a mathematically defined, three dimensional tissue space according to Beer's Law, using a fast ray-tracing algorithm. The resulting test images are adequately realistic, inexpensive, and reproducible at any desired resolution. They may contain precisely defined and localized abnormalities of unlimited subtlety. This approach provides a flexible, easy-to-use research tool to explore digital techniques in mammography, as well as a potential aid to training of radiologists in early breast cancer detection.

Key words: breast, computer simulation, imaging, mammography, phantom

Supported in part by Grant CA-62243 from the National Cancer Institute, Bethesda, Maryland, USA.

INTRODUCTION

Technology for digital image acquisition, processing, and storage is widely available and has the potential to supplant conventional film-based processes for radiologic image capture, display, and archiving in routine clinical practice. The resolution of digital radiography is fast approaching acceptable limits for many applications. Mammography, in particular may well have the highest resolution requirements in diagnostic radiology, owing to the need to detect subtle microcalcifications that can herald the presence of an otherwise cryptic early malignancy. Computer-based workstations for mammography are already being tested clinically. The trend toward digital techniques is supported by the increasing computer literacy of radiologists, the development of reasonably priced, high resolution video display terminals, and the rapid evolution of digital image capture technology, including charge coupled devices (CCD's) that are able to acquire high resolution radiographic images (at least 2000 x 2000 pixels, or about 0.1 mm x 0.1 mm pixel size).

As such technology is further developed for general clinical use, there will be a need for a wide variety of test images, containing precisely known normal structures and precisely defined abnormalities. Of particular importance in the testing and validation of new diagnostic imaging methods is the assessment of system sensitivity and specificity, where the "system" in question includes both a trained radiologist and the imaging technology under evaluation. The most definitive approach to this key issue is receiver operating characteristic (ROC) analysis, in which curves are generated describing the diagnostic "hit rate" for detection of a particular abnormality as a function of the false alarm rate. To compare the performance of observers using a modified or innovative imaging system with the performance of the same observers using conventional technology, it is necessary to gather performance data for a series of 100 or more test images, in which the abnormal versus normal state is known. In the case of clinical material, diagnostic truth can be determined *post hoc* by biopsy, subsequent clinical course, etc. Another approach is to establish truth by consensus opinion of board certified radiologists. Both approaches are relatively costly, tedious, and productive of limited numbers of test images having a desired abnormality.

The use of computer models emulating the physics of x-ray absorption by three dimensional tissue masses, positioned in a geometric workspace between a defined radiation source and a detector array, can provide a useful source of stylized, but physically realistic test images. The potential advantages of computer generated images, rather than actual clinical radiographs, are that

(1) the true normal/abnormal state of the images is known exactly, because the abnormalities are deliberately created and mathematically defined;

(2) the number of possible abnormalities is unlimited, and the nature, background, and context of the abnormalities can be systematically varied to determine under what circumstances perception and diagnostic performance are most and least influenced by particular digital display techniques;

(3) the cost of obtaining images for analysis, of any desired complexity and at any desired resolution, is minimal;

(4) for many psychophysical experiments, the complete clinical process of image acquisition, display, and interpretation can be simulated at a computer-based workstation for efficient, objective data collection and analysis; and

(5) the fundamental questions regarding the virtue of various digital radiographic techniques as aids to human perception and diagnostic performance can be answered quantitatively without exposing patients to additional radiation.

The breast is especially well suited to be modeled as a collection of simple spherical primitives, owing to its geometry and composition. This report describes a C-language program library capable of creating (1) realistic tumor-bearing mathematical phantoms of the breast and, in turn, (2) mammographic images of the phantoms. Anatomically realistic features of the phantoms include overall size, geometry, and compression in 3 dimensions. A detailed and realistic treatment of fat lobules, provides a suitably complex background for glandular structures of the breast. Glandular structures are modeled as branched tubules of anatomically realistic size, number and complexity, including lactiferous sinuses and terminal lobules. The models also include Cooper's suspensory ligaments, differing in geometry and orientation from the glandular elements, and optionally any of three types of tumors varying in size and surface contours.

Manipulation of control parameters for such phantoms allows facile modeling of physiologic changes, including hypertrophy or atrophy of glandular elements, or tumor growth from one examination time to the next. Visually realistic features of the simulated x-ray images of the mathematical phantoms include physically correct x-ray attenuation of fat, water, and microcalcifications for 25 keV photons, magnification factors based on source-target distances, and the capability to introduce known amounts of motion artifact, shot noise, fog or scattering, if desired.

This working paper describes algorithms for creating virtual mammograms for medical imaging research. The first computational task is to create a table specifying the sizes, densities, and center coordinates of superimposed spherical primitive masses, which together mimic many physical features of a tumor-bearing breast. These primitives specify the gross outlines and skin of the breast, the internal detail of fat lobules, the Cooper's ligaments, lactiferous lobules, ducts, and sinuses, and optionally any of three types of abnormal tumor. The table of spherical primitives collectively constitutes a mathematical phantom of the breast. The second computational task is to create a digital x-ray image of the phantom by ray-tracing.

METHODS

Modeling Normal Soft Tissues of the Breast

Breast models can be created easily from simple spherical primitives enclosed in a three dimensional rectangular work space, as shown in Figure 1 for a cranial-caudal view. First two large, concentric hemispheres, the outermost of non-fat (skin) density and the innermost of fat density, are defined. The water density layer is created by overwriting a sphere of water density with a concentric sphere of fat density, 1 mm smaller in radius. These large hemispheres are doubly truncated at the north and south poles by the limited dimensions of the work space, leaving the middle third, to simulate breast tissue flattened to 6 cm thickness between compression plates during mammographic examination. The remaining elements of the breast model are contained within the resulting truncated hemisphere. If desired, essentially flat sheets of water density skin can be added adjacent to compression plates; although these have negligible effect upon the final image and can be omitted.

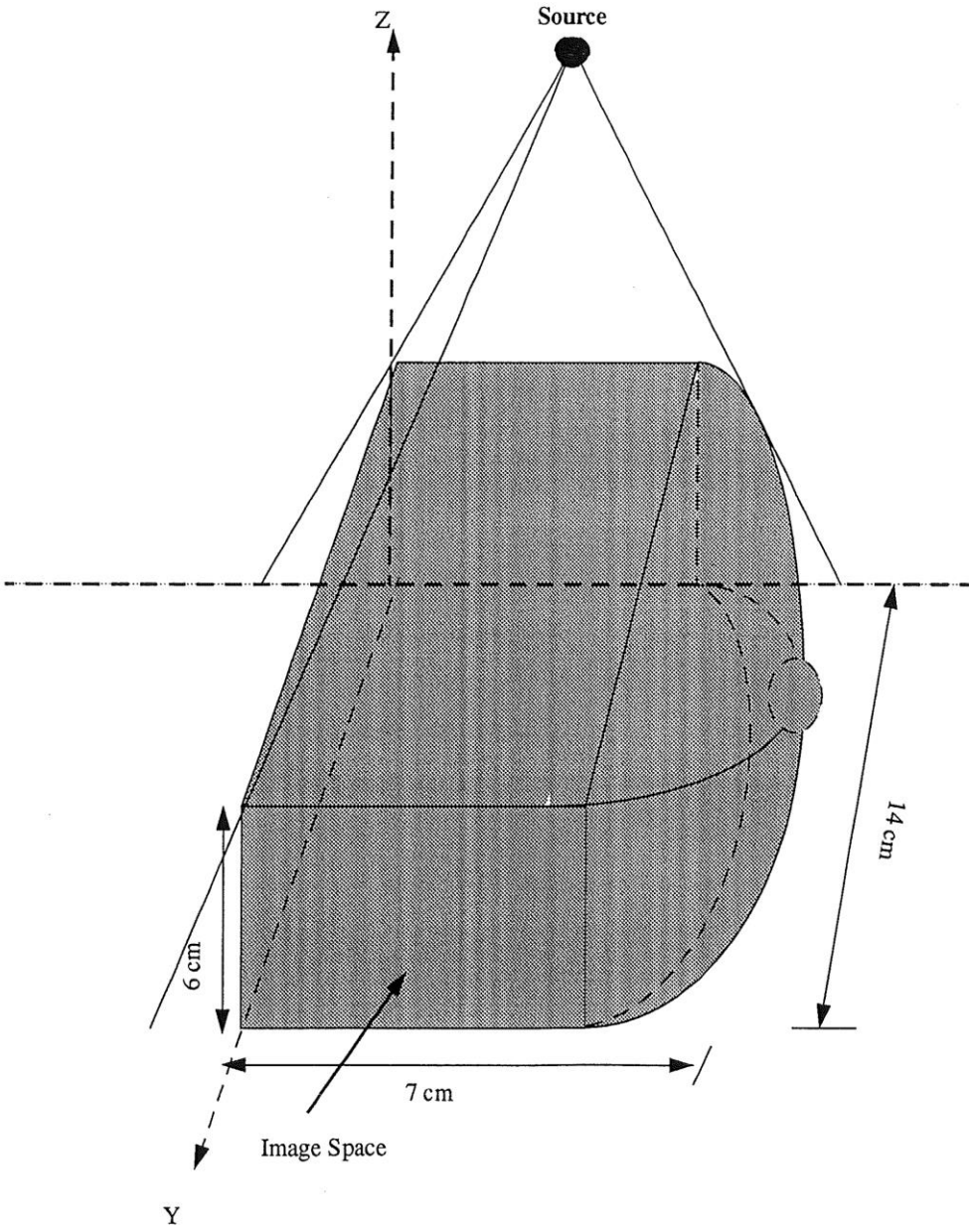

Fig. 1. Three dimensional rectangular work space for computational models of the breast. The computational phantom includes a breast-like hemisphere, 8 cm in radius, "compressed" by truncation to 6 cm thickness. The model work space has dimensions (x,y,z) of 8 x 16 x 6 cm, and is irradiated along the z-axis. Concentric hemispheres, centered at (0,8,3), represent non-fat density dermis and subcutaneous fat. Thousands of smaller, partially overlapping spherical densities are added to create detail of the subcutaneous fat and mammary gland parenchyma.

Correct modeling of the microscopic structure of adipose (fat) tissue is essential to obtain realistic looking computational models. Far from being a uniform and homogeneous fat density material, such as that present in the original fat density hemisphere, living adipose tissue of the breast is divided into lobules, embedded in a delicate meshwork of water density connective tissue, in which are found blood vessels that nourish the living fat cells. Thus fat lobules, averaging one half to one cm in diameter, are surrounded in vivo by interconnected sheets of supporting water density connective tissue. We model the microscopic connective tissue elements in fat tissue as a collection of thin, randomly placed, overlapping spherical shells of water density, surrounding the fat density cores. Fast, random number generators, validated for uniformly distributed random variables, are used to obtain random values when needed. The mean shell thickness, derived from microscopic examination of normal breast tissue is on the order of 0.02 cm. Random clusters of shells are created as pairs of very nearly concentric spheres--the second, slightly smaller, fat density sphere overwriting the first slightly larger water density sphere. In a typical breast model, 750 such pairs are created with a mean diameter of 0.5 cm. A small random variation in the center coordinates of each pair of spheres causes the shells to be other than perfectly uniform in thickness. Overlapping of the shells leads to an organic effect.

To further enhance the realism of background adipose tissue and to provide more diagnostically challenging simulated biologic variation of background density, we also include a slight regional variation in core fat lobule density. The anatomic concept underlying this variation is that in vivo fat lobules of approximately 0.5 cm in diameter are further penetrated by fine connective tissue strands, containing capillaries, which vary slightly in their number and arrangement. The presence of microscopic connective tissue elements within each macroscopic fat lobule is represented by a slight and variable increase in the core "fat" density. The core fat density is allowed to vary according to the following cosine function:

$$\text{Core density} = D_{\text{fat}} \cdot (1.0 + a \cdot \cos(x+\phi_x) + b \cdot \cos(y+\phi_y) + c \cdot \cos(z+\phi_z))$$

where D_{fat} is fat density, a, b, and c, are uniformly distributed random variables for each breast, ranging from 0 to 0.05, x, y, and z are normalized spatial coordinates, and the ϕ's are randomly selected phase angles. The small, 5% regional variation in fat lobule core density eliminates monotonous uniformity of background. With such variation, each of the hundreds of fat lobules in the breast can be convincingly modeled as a pair of outer water density and inner fat density primitives. These fatty elements are written prior to the subsequent addition of Cooper's ligaments, glands, ducts, and tumors, which become superimposed upon the background of the adipose tissue matrix.

Internal parenchymal structures of the breast are modeled as chains of telescoped spheres extending outward from the chest wall toward overlying skin. Cooper's ligaments are modeled as chains of partially overlapping constant diameter spheres, arising randomly at points near the chest wall and in the general direction of a perspective point outside the breast beyond the nipple. Random variation of the perspective point from ligament to

ligament gives an organic appearance to the array of ligaments. Glandular elements are modeled as chains of telescoped spheres arising from non-overlapping points near the chest wall and progressing either in the general direction of a randomly selected focal point within subcutaneous tissue deep to the nipple or, alternatively, in the direction of a neighboring duct to create a branch. The separation of the clusters of focal points for the ligaments and for the tubulo-lobular ducts creates a crisscross pattern of their respective radiographic shadows, similar to that observed in actual mammograms.

Along the length of the glandular chains, the diameter of component spheres is varied to create enlargements representing lobules at ends distal to the nipple and lactiferous sinuses at ends close to the nipple. Widening of the ducts in these regions is accomplished according to arguments of a function that specifies the length and width of the fusiform bulge in the duct chain (Figure 2).

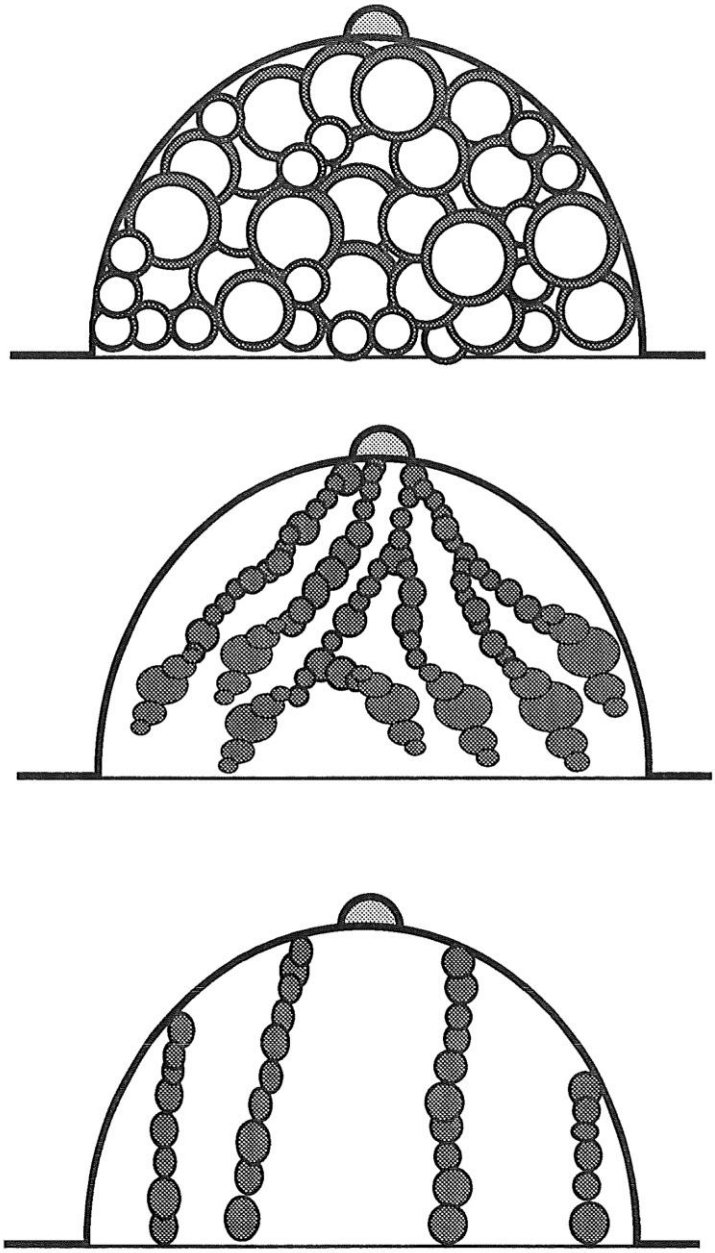

Fig. 2. Scheme for creation of soft tissues of the breast, including fat lobules, branched, lobulated ducts, and suspensory ligaments. Fat lobules are created as thin, water density shells, surrounding fat density cores. Glands are created as chains of partially overlapping spheres, grown from the base of the breast near the chest wall toward the nipple. Fusiform enlargements of chain elements constitute terminal lobules and lactiferous sinuses. All elements are schematic and enlarged for the purpose of illustration.

A branching pattern of glandular elements is created in conjunction with "backwards" growth of the glandular chains from the chest wall toward the nipple. Chain growth is accomplished by adding successive elements to the end of the chain that partially overlap the former terminal element. To encourage branch formation, the growing ends of the chains are attracted toward the nearest spherical element in a pre-existing duct, as well as toward the nipple. For this purpose, pre-existing ducts are distinguished from lobules or sinuses by their maximum diameter. When a growing chain meets an existing chain, they fuse, forming a branch and further retrograde growth of the tributary duct stops.

The direction of chain growth is determined by a linear combination of the unit spatial vector pointing from the growing chain end toward the near-nipple focal point and the unit spatial vector pointing toward the nearest pre-existing duct. The target site on the nearest duct to which the growing chain is attracted is updated after every 1 to 3 cm of chain growth. In this way more than one potential branch point is identified during chain growth, however the growing chain does not have to hit a moving target, but rather a stationary one at each successive level from chest wall to nipple. The proportions of the attraction rate to the nipple and to each potential branch point are determined by a user-specified branching factor. The greater the branching factor the greater the attraction toward a branch point and the less the attraction toward the nipple. Branching factors near 0.5 create anatomically normal branching patterns.

Typical anatomic variables, describing the numbers and diameters of lobules, ducts, and sinuses, were derived from the published literature. To model a lactating breast, one can increase the size of the lobules, ducts, and sinuses. During post-menopausal atrophy of the breast there is diminution, and ultimately, disappearance of glandular elements. Thus, to model an atrophic breast one can decrease the size and/or number of glandular elements.

Modeling Tumors of the Breast

In a final optional step of mathematical phantom creation, spherical or multi-nodular tumors can be incorporated into the digital phantom breast, with or without small clusters of microcalcifications--all by the geometric superposition of spherical masses of the desired size. Schemata for modeling 3 types of tumors are shown in Figure 3.

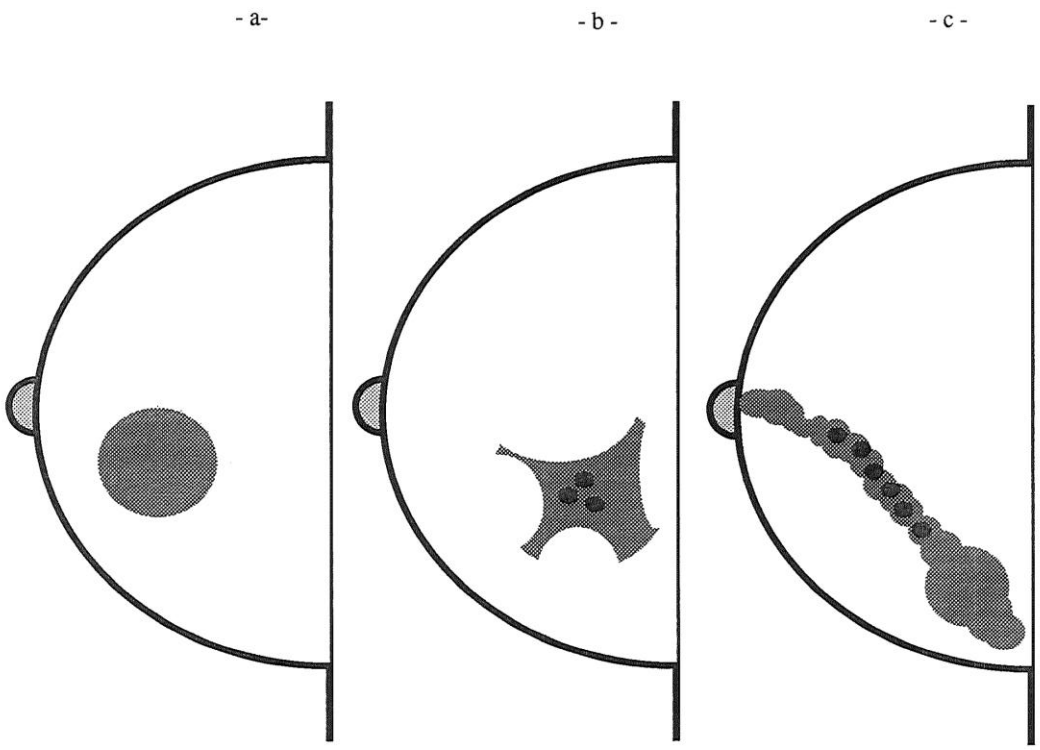

Fig 3. Schemata for modeling 3 types of tumors, enlarged here for clarity. (a) "fibroadenomas" are spherical enlargements of existing duct elements that push away nearby normal elements. (b) "invasive ductal carcinomas" are stellate masses, created by erosion of a larger central, water density sphere by overlapping smaller peripheral spheres of fat density. When the radii of the peripheral spheres are about 0.5 times that of the central sphere and when their number is about 20, then the residual water density object becomes cratered and spiculated in appearance, not unlike invasive cancer. (c) "intraductal carcinomas" are indicated by random microcalcifications within otherwise normal ducts.

Simple spherical or lobulated fibroadenomas of any size can be modeled by replacement of a randomly selected glandular element with a water density element of a larger diameter. This type of non-malignant, encapsulated tumor produces architectural distortion by pushing aside nearby normal tissues. The process of expansive displacement can be modeled by displacement of normal elements overlapped by the larger tumor mass in the direction of the unit vector pointing from the center of the tumor to the center of the displaced mass.

Invasive ductal cancers often have irregular shapes and spiculated borders. We have modeled these tumors beginning with a single water density mass, similar to the fibroadenoma, which is subsequently overwritten or eroded by superimposed peripheral fat density spheres. These are centered at random points 0.7r from the center of the original fibroadenoma-like mass, where r is the tumor radius. The diameters of the fat density overlays average 0.25r with standard deviation 0.2r. The more fat density spheres that are used to erode the surface of the tumor, the more irregular in shape it becomes.

Unlike fibroadenomas, invasive ductal cancers cause retractive architectural distortion in the opposite direction to expansive architectural distortion: nearby normal elements are drawn toward the malignant mass, owing to the contraction of scar tissue that forms around the tumor. This process of retractive architectural distortion is modeled by attraction of normal elements along a vector pointing from the center of the attracted mass toward the center of the tumor. In our current implementation, the amount of attraction varies inversely with distance from the tumor, so that nearby structures are more strongly attracted than those farther away. In clinical mammograms such architectural distortion can sometimes serve as a diagnostic clue to an otherwise cryptic malignancy.

Another visible sign of malignancy is the presence of suspicious, pleomorphic microcalcifications, which are variable in size, shape, and density, and which are distributed in clusters. Microcalcifications form in necrotic cells within tumor filled ducts or are actively produced by the tumor cells. To represent such calcifications, the locations of pre-existing normal ducts within the radius of the tumor are copied to the end of the list of added elements (so that they will not be overwritten by the tumor itself) and very small calcium density spheres (mean diameter 0.007 cm, SD 0.003 cm) of varying size, are placed at random sites within the lumens of the former normal ducts.

Intraductal cancer (ductal carcinoma in situ) is usually mammographically visible because of the presence of microcalcifications. To model intraductal cancers, we select at random a malignant focus in a continuous segment of a single duct (not a Cooper's ligament). Then elements along a selected and randomly varied length of the duct are impregnated with microcalcifications located randomly within the duct radius. X-ray images of the resulting structures closely mimic those of classical intraductal cancers.

The output of our phantom generation software is a table of the diameters, scaled densities, and center coordinates of spherical primitives. These primitives specify in order, the gross outlines and skin of the breast, the internal detail of fat lobules, the Cooper's ligaments, lactiferous lobules, ducts, and sinuses, and optionally any of three types of abnormal tumor. This table of primitives collectively comprises the digital phantom and is subsequently read by the x-ray image formation simulator. In routine use, operating system pipelines are used to link the output of phantom generation software to the input of the x-ray image simulator directly, without the use of intermediate files.

Creation of Simulated Mammograms by Ray Tracing

The general approach to computer simulation of radiographic images is shown in Fig. 4. Transmission images are computed using a ray-tracing algorithm (Glassner, Introduction to ray tracing, London 1989) for x-rays arising from a defined point source, passing through a simulated tissue volume, and striking an image plane, where a phosphor/film surface, charge coupled device (CCD), or other radiologic detector would be located. Objects in the scene consist of sets of overlapping spheres of varying size, density, and position. The sizes, densities, and center coordinates of successive spherical primitives, which constitute the digital breast phantom, are read as input, together with the dimensions of the work space and coordinates of the source. A window on the image plane borders one side of the workspace and is divided to the desired spatial resolution into a rectangular grid, the coordinates of which correspond to picture elements (pixels). The relative number of photons reaching any point in the image plane is computed using Beer's Law for absorption of photons by radiodense materials along chords produced by ray intersections with each spherical primitive, as shown in Figure 4.

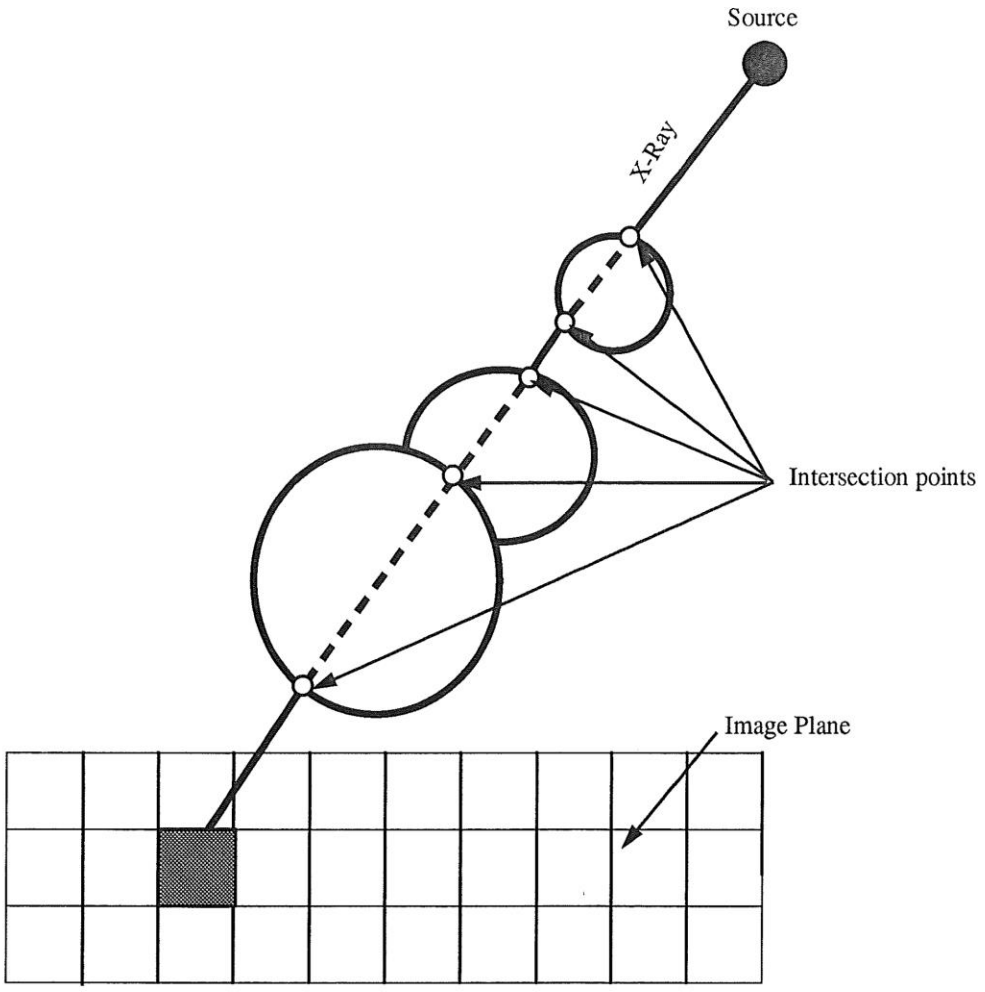

Fig 4. Approach to ray tracing for simulated x-rays. Rays are tested for intersection with a list of spherical primitives. Intersection points are calculated and sorted. Primitives appearing later in the list overwrite primitives appearing earlier in the list. Attenuation of ray intensity is computed by Beer's Law form the final sorted list of intersection points and the linear attenuation coefficients of corresponding primitives.

To perform the integration describing x-ray transmission through each phantom, The radiation transmission from the source through each tissue element, beginning closest to the source and ending at each indexed pixel, is computed using the expression: $I = I_0 e^{-\mu L}$, where I is the number of transmitted photons exiting the object, I_0 is the number of incident photons entering the object, μ is the linear attenuation coefficient, and L is the length of the ray path through the object. For economy of language in the following discussion, the term "density" is often used as a synonym for the "linear attenuation coefficient", μ , in describing the properties of tissue models.

The general structure of the ray-tracing program is as follows:

```
read workspace dimensions, source coordinates, and properties of added masses
that constitute the "digital phantom"

for(each primitive mass density) {

        find pixels in current band shadowed by the mass and record ray-target
        hits in pixel-indexed hit list
}

for(each pixel) {

        if(hit list is empty) {

                write zero /* no shadows here */
        }

        else {/*do ray-tracing*/

                make unsorted scratch table of all ray-mass intersection points sort
                table of intersections by distance from source

                define sequential line segments for integration along ray from
                source to pixel compute transmission image brightness for pixel
                by Beer's law

                write brightness value for pixel
        }
}
```

The ray tracing algorithm includes three sets of tasks. (1) pre-computation of a pixel-indexed list of spheres intersected by rays extending from the source to each pixel, and (2) computation of ray-sphere entry and exit points, sorting of the ray segments traversing intersected spheres, and finally (3) application of Beer's law along the ray path. An advantage of the ray-tracing approach is that the number of calculations required by a ray tracing algorithm is proportional to the number of pixels--i.e. the image plane area, not the volume of the tissue model. Thus the execution time is roughly proportional to the image resolution squared, rather than to the resolution cubed.

Clever pre-computing of ray-object "hits" makes for fast overall performance. Our approach is to find pixels shadowed by each spherical mass and keep a list of the masses shadowing each pixel. The outline of the shadow of each spherical mass is found exactly by solving the ray-sphere intersection test equation for rays just tangent to the sphere (discriminant = 0). To save time only the outline of the shadow is computed. The hit list for each pixel within the shadow is then augmented by the address of the shadowing sphere. In this way all objects shadowing each pixel are recorded.

After creation of the hit list, ray tracing is performed. For each shadowed pixel the ray tracing module finds actual entry and exit points of each intersected mass in terms of the distance from the source along the ray path. This distance is clipped at boundary planes of the tissue volume, z = 0 and z = zheight. Ray distances, mass densities, and other needed values are stored in an unsorted data structure and then sorted by ray distance, closest to farthest from the source. Sequential line segments for Beer's law are derived, incorporating an overlay feature, in which successive overlapping primitive masses in the input stream replace prior masses in the tissue model, as shown in Figure 4. This paint-over feature is especially useful in sculpting anatomically realistic models with simple spherical primitives. For each pixel in the final image, the ray tracing routine returns a transmission image value, proportional to the percent of incident photons reaching the image plane. For medical images this value is inverted to create an·absorption image in which brightness is an indicator of intervening structures that absorb x-rays.

Simulation of Film Processing

The image computed by Beer's Law can be thought of as the analog of the latent image captured in exposed, undeveloped film, or even more straightforwardly, the set of values captured by an array of charge coupled devices. In practice, radiographic technique (kVP and mAs), choice of film, and conditions of development are adjusted through trial-and-error to create a visible image, in which clinically relevant information is centered in a gray scale ranging from nearly black to nearly white. In using computational phantoms, this process is simulated by simple linear transformation of raw image values, or "histogram stretching", such that the gray scale values of interest in the image are distributed over the black-to-white range of the final display device, such as a printer or video screen. For example, if the printer can display 256 gray levels, specified by integer values, then the double precision floating point values of the raw image are scaled and stretched to span the range 0 to 255, and the test image is written and stored in 8-bit binary words. (The roughly linear relationships between x-ray film exposure and the optical density of the developed radiograph, and in turn between optical density and the physiologic response of the eye to light have been discussed by Meredith and Massey (Fundamental Physics of Radiology, Second Edition, Williams and Wilkins, Baltimore, pp. 66-181). Using such linear scaling, one may readily obtain images that are similar in contrast to clinical mammograms.

RESULTS

Validation

The algorithm for creating mathematical models was validated by reference to the published literature describing the gross and microscopic anatomy of the human breast and the physical properties of breast tissues. Sizes and dimensions of glandular elements were selected with reference classic anatomy texts to the detailed morphologic studies of Vorhen (The Breast, 1974) Scaled literature values of linear attenuation coefficients for 25 keV photons (recommended for mammography) in soft tissues of the breast are utilized in the computational phantom: 0.32 cm^{-1} for fat, 0.51 cm^{-1} for non-fat (water density), and 0.53 cm^{-1} for tumor (F. A. Duck Physical Properties of Tissue, 1990).

The C-language code for creating two-dimensional transmission images was validated by analysis of the size and position of shadows cast by standard test spheres placed at various known locations and irradiated from various perspectives. Computed results were compared to those expected from geometric calculations, with good agreement within the limits of resolution tested.

Normal images

Figure 5 illustrates normal tissue components of complex computer simulated mammograms derived from a mathematical, computer model containing a breast-like hemisphere 8 cm in radius and "compressed" by truncation to 6 cm thickness. The x-ray source was located 60 cm above the distal edge of the breast model, at which was located the image plane. The raw transmission image was subjected to a linear histogram stretch to achieve contrast similar to that in clinical mammograms. In Figure 5(a) skin and fat lobules are included without lactiferous ducts and glands and without any tumor mass. Image (a) illustrates the pattern of lobulated background fat that constitutes the bulk of breast tissue. In Figure 5(b) glandular lobules have been added in an interconnected, branched pattern, superimposed upon the same tissue matrix of fat lobules as is imaged in Figure 5(a). Multiple secondary ducts converge in three dimensions upon the primary ducts. In addition there are Cooper's ligaments, which are not branched.

In the model of Figure 5(b) the diameters and numbers of glandular elements have been selected to reflect the anatomy of a postmenopausal woman. The relative preponderance of fat density provides a relatively radiolucent background for tumor detection. In the model of Figure 5(c) additional glandular elements have been added, and the water density rims of supporting connective tissue surrounding fat lobules have been thickened to represent an estrogen stimulated, dense breast of a pre-menopausal woman, in which radiographic detection of tumors is more difficult owing to the larger proportion of water density structures in normal background tissues.

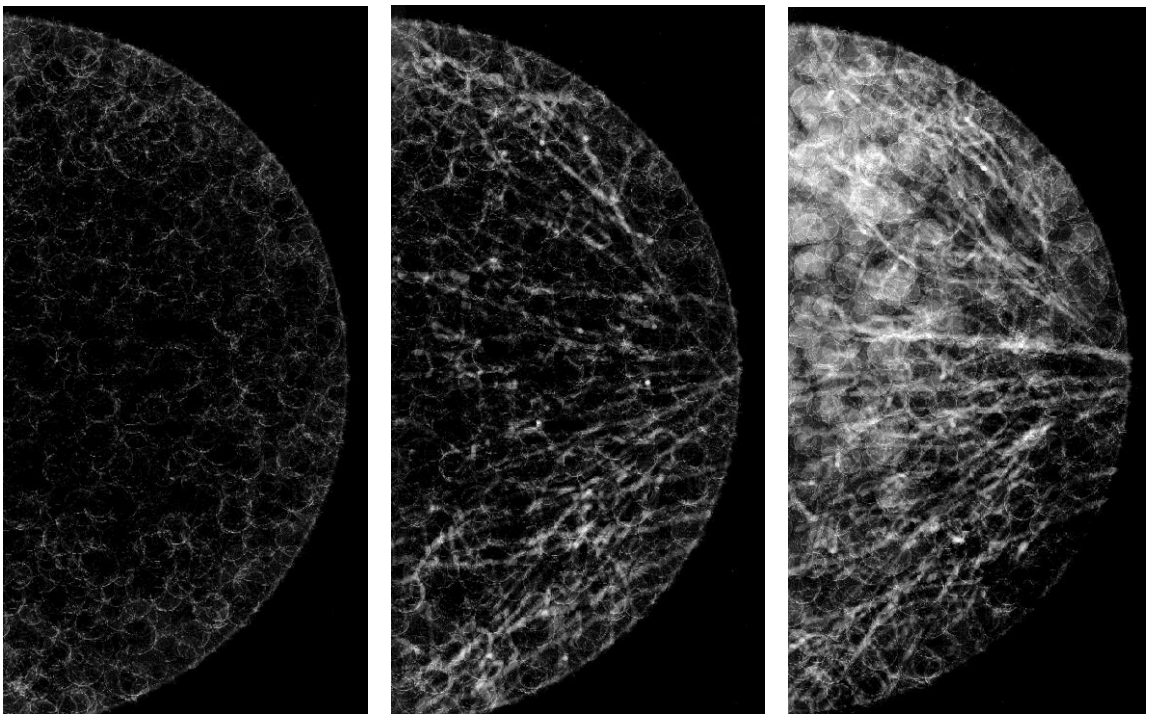

(a) (b) (c)

Fig 5. Simulated mammogram of normal breast tissues. (a) skin and fat only (b) glandular elements and Cooper's ligaments added (c) model of dense breast with hyperplasia of microscopic connective tissue elements within fat lobules

Tumor images

Figure 6 illustrates computational models of three types of tumors: a fibroadenoma, an invasive ductal carcinoma, and an intraductal carcinoma. In Figure 6(a) an obvious 0.5 cm diameter spherical fibroadenoma is modeled. This tumor was created by enlarging a single primitive element comprising a pre-existing duct. Expansive architectural distortion was included by displacement of Cooper's ligaments and glands away from the center of the growing tumor. The amount of displacement is sufficient to prevent overlap of the tumor with the displaced normal structures, as occurs in the natural history of these benign lesions.

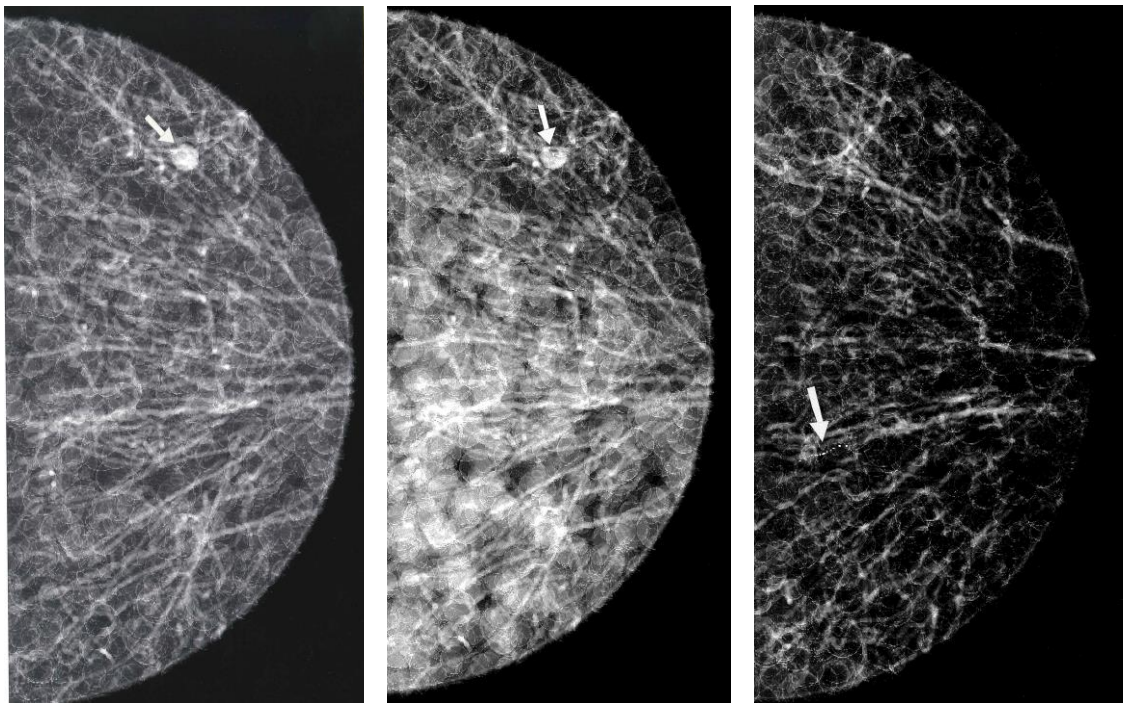

(a) (b) (c)

Fig 6. Computational models of three types of tumors in computational breast phantoms: (a) a fibroadenoma, (b) invasive ductal carcinoma, (c) intraductal carcinoma.

An invasive ductal carcinoma with associated microcalcifications is illustrated in Figure 6(b). The spiculated mass was created by erosion of a spherical density by multiple peripheral spheres of background (fat) density, as sketched in Figure 4. This arrangement was subsequently overlaid by microcalcifications randomly placed along the length of pre-existing lactiferous ducts that have been enveloped by the tumor. Retractive architectural distortion was included by causing nearby elements of Cooper's ligaments and glands to be attracted toward the center of the growing tumor, mimicking the effects of contraction of scar tissue that has formed around the tumor, perhaps in response to tumor-produced growth factors. Normal tissue elements within the tumor radius, however, are not displaced outward, in order to reflect the invasive nature of malignant cancers.

In Figure 6(c) a 1.0 cm long intraductal carcinoma is shown. This tumor was created by enlarging preexisting water density ducts and adding random microcalcifications along the course of the original lumen. Such cancers are a form of carcinoma in situ and continue to be oriented in the same spatial direction as the original pre-malignant duct. Here the major diagnostic sign is the presence of microcalcifications, without which, the lesion would be often missed.

DISCUSSION

Using overlapping spherical masses to create a computational phantom of the breast, it has proved easy to sculpt test images of three dimensional ductal-lobular glands and Cooper's ligaments embedded in lobulated fatty tissue that seem sufficiently anatomically realistic for many research applications. Digital phantoms are inexpensive, safe, flexible, precisely defined, and reproducible. A large number of exactly known abnormalities of varying conspicuity can be included. In principle, digital images of any desired spatial resolution or gray scale resolution can be created. Our current software, sample control files, and any future upgrades will be made freely available to colleagues as C-language source code via electronic mail.

The present breast phantom based upon spherical primitives has a large number of realistic features, including overall three dimensional size and shape, inclusion of water density and fat density components of adipose tissue, random and complex trees of branched ducts terminating in lobular glands, together with interspersed suspensory ligaments. Tumors of three different anatomic types and any desired size can be caused to arise from glandular or duct elements (not ligaments). The parameters defining the non-fat elements of the phantoms can be changed to mimic life cycle changes in their growth and involution.

In the present project we were surprised to note the degree of complexity and realism achievable with combinations of simple spherical primitives. A few minor non-realistic features remain. The skin facing the compression plates (which introduces negligible background attenuation to the final image) is either omitted or alternately modeled as thin tangential slice of a large radius sphere external to the tissue space, in which case it is not of uniform thickness. A commonly seen feature in actual mammograms of older women is the presence of calcified blood vessels, which are not presently modeled. These vessels do not produce diagnostic problems, because they are readily identified, and so have been omitted for the sake of simplicity. The only anatomically significant limitation of the present model is that larger planar septae (like those of a grapefruit) that separate lobes of actual parenchymal tissue in the breast are not represented as water density sheets in three dimensions, but instead are represented as cords. The shadows of "Cooper's ligaments" in actual mammograms are likely images of septae viewed end-on, such that the effective thickness of water density in the ray path is great. These septae might be well appreciated in one view but not in another; whereas cord-like structures in our models extending from the chest wall to the nipple would appear in any view. In this sense the virtual mammograms described herein are less variable in appearance from one examination or view to another than would be actual mammograms. The very large number of smaller connective tissue septae that surround fat lobules, however, are modeled and give a finely reticulated background density very similar to that of most regions of subcutaneous fatty tissue in the breast.

The forgoing limitations notwithstanding, the simple virtual mammograms described herein can provide valuable and cost-effective alternatives to actual mammograms for many purposes in both research and clinical training. Potential applications include their use as research tools, which can be applied to studies of image enhancement techniques such as edge detection, histogram stretching, contrast enhancement, etc. It is also possible to model and study degradation of images by various forms of noise or by patient motion, the artifacts of which can be readily introduced into digital images. In such research applications the use of computational phantoms also permits comparison of test images with the known three dimensional density map of x-ray absorbers from which the images were generated. Various figures of merit for comparing alternative display methods can be computed on the basis of the correlation of the test images with the actual densities present.

Another family of possible applications for such computational phantoms includes their use in the training of radiologists. In this application virtual mammograms with known abnormalities are interpreted by students, either during practice sessions or during testing. Such images can be displayed on video terminals, or copied onto conventional film. A classical advantage of computer aided instruction as a supplement to traditional methods of instruction is that training modes can be made interactive, such that the presented images and their degree of difficulty are selected according to the trainee's correct or incorrect responses. When implemented properly, such branching algorithms for computer aided instruction, which pose problems and respond according to the students' previous decisions, maximize learning rate and minimize boredom, allowing each trainee to be optimally challenged.

Depending on the computational speed and storage media available, test images could be either generated on-line or selected from a pre-existing library. Additional features of computer assisted radiological training could readily include incorporation of hints, by which learners are assisted in difficult cases, incorporation of help, wherein certain general rules are reviewed, the ability to zoom the generated image to focus on finer detail in a targeted region, and automatic record keeping and collection of performance statistics. Although early versions of computational phantoms for use in computer aided instruction would be developed by teams including both board certified radiologists and competent computer programmers; advanced versions could be supported by "authoring programs" that allow the non-programming instructor to create a variety of lessons, incorporating desired normal and abnormal anatomical features. Accordingly, we envision widespread future application of computational phantoms in academic radiology, both for research and for training in breast cancer detection.